LANGMUIR

Article

pubs.acs.org/Langmuir

Brownian Dynamics of Electrostatically Adhering Small Vesicles to a Membrane Surface Induces Domains and Probes Viscosity

Seyed R. Tabaei,[†,‡] Jurriaan J. J. Gillissen,[†,‡] Min Chul Kim,[†,‡] James C. S. Ho,[†,‡] Bo Liedberg,[†,‡] Atul N. Parikh,[†,‡,§] and Nam-Joon Cho*[,†,‡,∥]

[†]School of Materials Science and Engineering, Nanyang Technological University, 50 Nanyang Avenue 639798, Singapore

[‡]Centre for Biomimetic Sensor Science, Nanyang Technological University, 50 Nanyang Drive 637553, Singapore

[§]Department of Biomedical Engineering and Department of Chemical Engineering and Materials Science, University of California, Davis, California 95616, United States

[∥]School of Chemical and Biomedical Engineering, Nanyang Technological University, 62 Nanyang Drive 637459, Singapore

Supporting Information

ABSTRACT: Using single-particle tracking, we investigate the interaction of small unilamellar vesicles (SUVs) that are electrostatically tethered to the freestanding membrane of a giant unilamellar vesicle (GUV). We find that the surface mobility of the GUV-riding SUVs is Brownian, insensitive to the bulk viscosity, vesicle size, and vesicle fluidity but strongly altered by the viscosity of the underlying membrane. Analyzing the diffusional behavior of SUVs within the Saffman−Delbrück model for the dynamics of membrane inclusions supports the notion that the mobility of the small vesicles is coupled to that of dynamically induced lipid clusters within the target GUV membrane. The reversible binding also offers a nonperturbative means for measuring the viscosity of biomembranes, which is an important parameter in cell physiology and function.

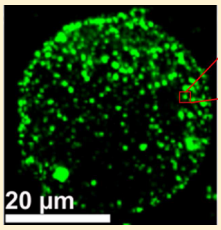

INTRODUCTION

A single lipid membrane—a flexible, quasi-two-dimensional biomolecular surface composed of two apposing layers of amphiphilic lipids[1]—fluctuates freely in water.[2] As two membranes come into close proximity, their thermally excited, out-of-plane fluctuations become suppressed, giving rise to a long-range repulsive force that tends to drive the membranes apart.[3] Overcoming this entropic repulsion, such as through biospecific ligand−receptor binding or nonspecific electrostatic attraction between oppositely charged membranes, can bring membranes together, creating distinct adhesion configurations or intermembrane junctions.[4] Such junctions are not uncommon in biology. They represent an integral part of intercellular signaling strategies used by multicellular organisms,[5] among which perhaps the best known example is that of an immunological synapse. Here, single T-cells come into a junction with single antigen-presenting cells characterized by a molecular pattern of adhesive bonds consisting of central clusters of T-cell receptors surrounded by a ring of adhesion molecules.[6]

Beyond the suppression of thermal undulations, the appearance of intermembrane adhesive states introduces additional physical perturbations into the interacting membranes,[1] with important ramifications. Previous efforts, focused dominantly on the adhesion of membranes of comparable dimensions, document processes of adhesion-induced changes in membrane physical properties. A variety of features, including adhesion-induced changes in membrane tension, lateral fluidity, spatial distributions of membrane molecules,[7] and chemically differentiated domains[8] within single membranes as well as the exchange of lipids between interacting membranes,[9] have all been reported. Between membranes interacting through weak electrostatic forces, a notable example is the emergence of an adhesion gradient through molecular redistributions of charged amphiphiles. Here, the induced charge gradient acts to propel the vesicle along the gradient reconstituting the so-called haptotaxis observed in living cells.[10]

In the same vein, studies aimed purportedly at characterizing intermembrane junctions involving membranes of vastly different dimensions are much more limited. In living cells, such junctions appear transiently as prefusion or postdivision docking states during endo- and exocytosis, transporter vesicle morphogenesis, and viral budding and egress.[11] At the morphological level, they are perhaps best represented by closely apposed nanoscopic, colloidal (∼50−100 nm in diameter) small unilamellar vesicles (SUVs) and a target, 10−50-μm-diameter giant unilamellar vesicle (GUV). In this situation, a population of small vesicles adhering to and surfing on (in the case of weakly adhering membranes) a membrane produces a dynamic array of intermembrane junctions creating local and mobile hot spots. Similar localized hot spots, created through the hybridization of single DNA tethers between lipids of SUVs and solid supported membranes, have been previously shown to significantly impact diffusion.[12] They reduce the lateral diffusivities of the surfing SUVs and thus the DNA-lipids in supported membranes by 3- to 5-fold, which was speculated

Received: March 12, 2016
Revised: May 5, 2016
Published: May 10, 2016

DOI: 10.1021/acs.langmuir.6b00985
Langmuir 2016, 32, 5445−5450

to reflect changes in the local environment of tethering DNA lipids, which effectively increases the size of the diffusing components in the supported bilayer. This multiple tethering effect can be expected to be much more pronounced when SUVs adhere to GUV membranes electrostatically. In that situation, a large adhesion zone, determined by the size of the SUVs, can be expected to cluster a number of underlying lipids in the GUV membrane, affecting both the SUV mobilities and splitting the lipids in the GUV between two subpopulations: free lipids moving individually and clusters or discs of lipids whose concerted mobilities determine the translational diffusivities of the riding SUVs.

In the work reported here, we track the motion of individual electrostatically adhering SUVs riding onto the GUV surface, which serve as a probe to measure the viscosity of the underlying membrane. This membrane viscosity has been proven difficult to measure, and various techniques have been developed in the literature. An interesting recent technique uses a relation, which is calibrated in the bulk, between the viscosity and the emission of fluorescently labeled molecules incorporated into the membrane.[13] Another novel approach measures the shear-induced, large-scale circulation within the membrane of a GUV attached to the wall of a flow chamber.[14] Most methods, however, rely on measuring the diffusivity of tracer particles embedded in or adhering to the membrane and invoking a fluid mechanics model to translate the diffusivity to viscosity. For instance, the mobility of membrane lipids or membrane proteins has been measured using fluorescence recovery after photobleaching[15] or fluorescence correlation spectroscopy.[16,17] Translating diffusivity to viscosity, however, using fluid mechanics models generally works better for larger particles than for individual molecules. Therefore, in an attempt to accurately determine the viscosity of lipid bilayers, single-particle tracking has been used to measure the diffusivity of large membrane inclusions, such as phase-separated lipid domains[18,19] or peripherally bound tracer particles, using covalent bonds.[12,20−22] This latter approach is complicated by the unknown effective size of the diffusing objects, owing to an uncontrollable number of bonds and a possible deformation of the underlying membrane. Here, we circumvent these problems by using a weak electrostatic force to bind small vesicles to the membrane. We will show below that the vesicles associate with a cluster of membrane lipids and that the radius of the diffusing cluster correlates well with the electrostatic adhesion zone, permitting a straightforward determination of the membrane viscosity.

MATERIALS AND METHODS

GUV Preparation. Giant unilamellar vesicles (GUVs) were prepared using the electroformation method.[23,24] Briefly, stock solutions of lipid mixtures (mol/mol) were prepared at 1 mg/mL in chloroform. (All lipids were purchased from Avanti Polar Lipids.) Twenty microliters of the stock solution were spread onto the conductive side of ITO-coated slides within an area delimited by an O-ring and allowed to dry in vacuum for at least 1 h. Electroformation was performed with a 300 mM sucrose solution by using a commercial Vesicle Prep Pro (Nanion, Munich, Germany). Specifically, DOPC (1,2-dioleoyl-*sn*-glycero-3-phosphocholine)/DOEPC [1,2-dioleoyl-*sn*-glycero-3-ethylphosphocholine (chloride salt)] (9:1), DOPC/cholesterol/DOEPC (5:4:1), and DMPC (1,2-dimyristoyl-*sn*-glycero-3-phosphocholine)/DOEPC (9:1) GUVs were electroformed by applying an ac current at 500 Hz, 3 V, and 45 °C (above the gel−fluid transition temperatures of the lipid mixtures) for 120 min. Then the GUVs were diluted in a 300 mM glucose solution. Experiments involving DOPC/DOEPC GUVs were also performed in a more viscous solution. For this purpose, 25% (v/v) glycerol was added to the external bath in which the GUVs were diluted. Upon glycerol addition, the GUV underwent shrinkage due to an osmotic imbalance. However, because the permeability of the membrane to glycerol is relatively high (~2 × 10^{-6} cm/s),[25] the GUV regained its initial spherical shape a few minutes later, after yielding iso-osmotic conditions. Therefore, SUVs were added 30 min after the addition of glycerol to ensure complete equilibrium.

SUV Preparation. Small unilamellar vesicles (SUVs) were made by the extrusion method. Briefly, a mixture of DOPC and DOPS [1,2-dioleoyl-*sn*-glycero-3-phospho-L-serine (sodium salt)] (5 mol %) in chloroform was prepared at a total lipid concentration of 5 mg/mL. Rhodamine-DOPE (1,2-dioleoyl-*sn*-glycero-3-phosphoethanolamine-*N*-(lissamine rhodamine B sulfonyl) (1 wt % in chloroform) was also included. (All lipids were purchased from Avanti Polar Lipids.) The lipid solution was first dried using a flow of nitrogen. The dried lipid film was stored in vacuum for 3 h, after which it was rehydrated with buffer (Tris 10 mM, NaCl 150 mM, pH 7.5). After vortex mixing of the solution of hydrated lipids, unilamellar vesicles were made with an Avanti Mini-Extruder (Avanti Polar Lipids) using a polycarbonate membrane (100 nm pore size, Avanti Polar Lipids). The vesicle size distribution was measured by the Nano-Sight particle tracking technique (NanoSight, U.K.).[26]

GUV and SUV Mixing. After electroformation, 10 μL of the GUV solution was mixed with 200 μL of a 300 mM glucose solution in the μ-Plate 96-well (Ibidi, GmbH, Germany) for microscopy imaging. SUVs (5 mg/mL) were prediluted to 0.1 mg/mL in buffer (Tris 10 mM, NaCl 150 mM, pH 7.5), and 4 μL of this solution was added to the 200 μL GUV solution in the μ-Plate 96-well such that the SUVs sparsely decorate the GUVs. The pH and the ionic strength (NaCl) in the final solution were about 7.5 and 4 mM, respectively.

Fluorescence Microscopy. Spinning disk confocal microscopy measurements were carried out using an inverted Eclipse TE 2000 microscope (Nikon) fitted with an X-Light spinning-disk confocal unit (CrestOptics, Rome, Italy) and an Andor iXon+ EMCCD camera (Andor Technology, Belfast, Northern Ireland). For measurements, we used a 60× oil immersion objective (NA 1.49), and Rhod-DOPE (Ex/Em = 560/583) was exposed with a 50 mW 561 laser line. Time-lapse images were acquired at 50 frames/s. At least five GUVs were imaged for each experiment.

RESULTS AND DISCUSSION

Our experimental design involves the creation of a pericentric SUV−GUV interface stabilized by electrostatics (Figure 1a). We used negatively charged SUVs (~120 nm diameter) consisting of 95 mol % zwitterionic DOPC doped with 5 mol % negatively charged DOPS and positively charged GUVs

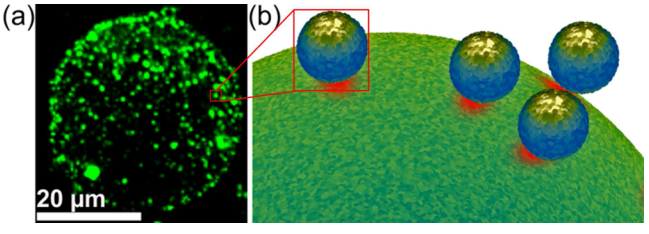

Figure 1. (a) Three-dimensional reconstruction from a stack of confocal cross sections of a GUV consisting of binary lipid mixture composed of DOPC and DOEPC (9:1) covered with SUVs (radius ~60 nm) composed of DOPC and DOPS (95:5) and doped with Rh-PE (1 mol %). (b) Schematic representation of electrostatically adhering small vesicles on the outer surface of a giant vesicle. The weak electrostatic tethering reversibly divides the membrane into two distinct subpopulations, i.e., free lipids and lipids in clusters (red regions) that are bound by the SUVs.

DOI: 10.1021/acs.langmuir.6b00985
Langmuir 2016, 32, 5445−5450

consisting of 90 mol % zwitterionic DOPC doped with 10 mol % positively charged DOEPC. At these low charge densities, the SUV−GUV interface is stable, showing little tendency toward intermembrane fusion, consistent with previous studies that have shown that the lower charge density threshold for fusion is roughly 10 mol %.[10,27] Moreover, to minimize the complicating effects of any molecular exchange and the creation of adhesion gradients at the SUV−GUV interface, we limit our measurements of SUV diffusion to the first several minutes after SUV adsorption, during which molecular exchanges are known to be minimal.[28] On these experimental time scales, we do not observe noticeable changes in the number of adhering vesicles, which confirms the irrelevance of intermembrane lipid mixing and/or fusion.

The diffusivity of vesicles was measured using a particle tracking method.[29] Previously, this approach has been used successfully to characterize the motion of nanoparticles,[30,31] peptides,[32] and viruses[33] at the membrane interface. To trace the 2D diffusive motions of vesicles, the equatorial plane of a GUV was imaged using confocal microscopy (Figure 2a). Using

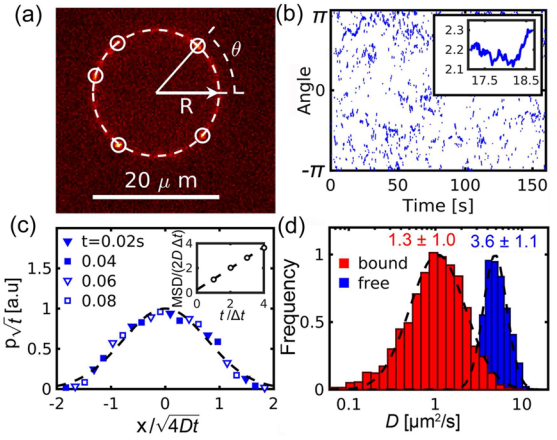

Figure 2. Mobility analysis of single small unilamellar vesicles (SUVs) diffusing on the surface of a giant unilamellar vesicle (GUV). (a) Image processing including the detection of the GUV edge at the equatorial cross-section (indicated by the dashed circle) and bound SUVs that appeared as bright spots on the GUV rim (marked by circles). An angle θ was assigned to each vesicle position at each frame. (b) Detected trajectories of bound SUVs on the (angle, time) plane at a temporal resolution of 20 ms. The inset shows a vesicle trajectory spanning about 2 s or 100 frames. (c) Displacement (x) probability (p) of surface-bound vesicles as a function of the normalized displacement $x/(4Dt)^{1/2}$, where D is the diffusivity and t is time. The dashed line is a Gaussian function. The inset shows that the mean square displacement (MSD) increases linearly with time, which indicates that the motion is Brownian. (d) Histograms of the diffusion coefficient D for surface-bound vesicles (red bars) and freely floating vesicles (blue bars). Note the logarithmic x axis.

in-house image analysis software (developed in MATLAB), the GUV rim (dashed circle in Figure 2a) and the SUVs (marked by circles in Figure 2a) were detected and vesicle trajectories along the equatorial GUV rim were constructed from a sequence of typically 10^4 images. After a vesicle moves into the confocal plane, its motion can be tracked only for a short while (typically 1 s) before it randomly moves out of the plane. Typically ~100 SUVs reside on the GUV surface (diameter ~20 μm), which is equivalent to an average distance between the SUVs of ~4 μm. Because this distance is much larger than the SUV diameter (~100 nm) and the Debye length (~1 nm), steric and electrostatic interactions between the SUVs are negligible. It is noted that for illustration purposes the GUV in Figure 1a had a relatively large SUV coverage whereas the SUV coverage in the diffusivity experiments was much lower.

Figure 2b shows the detected positions of the SUVs, expressed using the angle (θ in Figure 2a) along the equatorial GUV rim, as a function of time t. Because the SUVs continuously move in and out of the confocal plane, the trajectories in Figure 2a appear to be fragmented. An analysis of the mean square displacement (MSD) of the trajectories confirmed the Brownian character of the diffusion of the surface-bound vesicles (Figure 2c). Figure 2d presents a histogram of the diffusion coefficients for the surface-bound vesicles (red bars) as well as for vesicles freely floating in the bulk. The latter is obtained from vesicle tracking in the bulk using nanoparticle tracking analysis NTA; see Supporting Information Figure S2. The large spread in the diffusivity has many possible causes, e.g., measurement noise, distribution of vesicle sizes and charge densities, and statistical fluctuations due to the stochastic nature of the diffusional motion and the relatively short time that this motion can be sampled before the SUV moves out of the focal plane. We observe that the logarithm of the diffusivity is normally distributed (dashed lines), which means that the diffusivity itself is log-normally distributed.

The diffusion coefficient D for surface-bound vesicles is determined to be 1.3 ± 1.0 $\mu m^2\ s^{-1}$. With a radius of a = 57 ± 18 nm, which was measured using NTA (Supporting Information, Figure S2), the diffusivity of the freely floating vesicle equals 3.6 ± 1.1 $\mu m^2\ s^{-1}$, which is 3 times as large as that for the adhering SUVs. The smaller diffusivity for the adhering SUVs reflects a larger friction. To characterize the nature of this friction, we conduct a series of control experiments in which we study the influence of various membrane and solvent properties on SUV diffusivity on the GUV surface. The reader is referred to Table S1 and Figure S1 in the Supporting Information, which summarizes the SUV diffusivity and the displacement statistics for these control experiments.

We begin by analyzing the effect of the GUV membrane fluidity on the SUV diffusivity. For this purpose, we measure the SUV diffusivity on GUVs consisting of a mixture of 50 mol % DOPC, 10 mol % DOEPC, and 40 mol % cholesterol. Upon adding cholesterol to the underlying membrane, the SUV diffusivity is observed to decrease by a factor of 2 from 1.3 ± 1.0 to 0.6 ± 0.4 $\mu m^2\ s^{-1}$ (Figure 3a). This relative decrease is of a similar magnitude to that observed upon adding 40 mol %

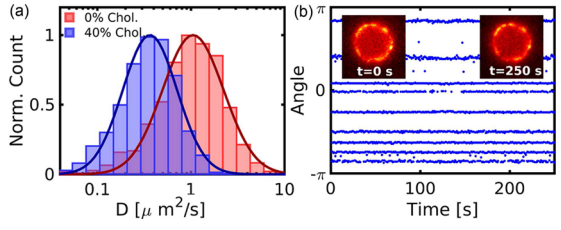

Figure 3. Effect of membrane properties on SUV diffusivity. (a) Histograms of diffusion coefficients D for surface-bound SUVs before (red bars) and after (blue bars) adding 40 mol % cholesterol to the underlying GUV membrane. The addition of cholesterol is seen to slow down the diffusional motion of the vesicles. Note the logarithmic x axis. (b) Trajectories of SUVs on a gel-phase GUV. The horizontal lines on the (angle, time) plane indicate that the SUVs are not moving.

DOI: 10.1021/acs.langmuir.6b00985
Langmuir 2016, 32, 5445−5450

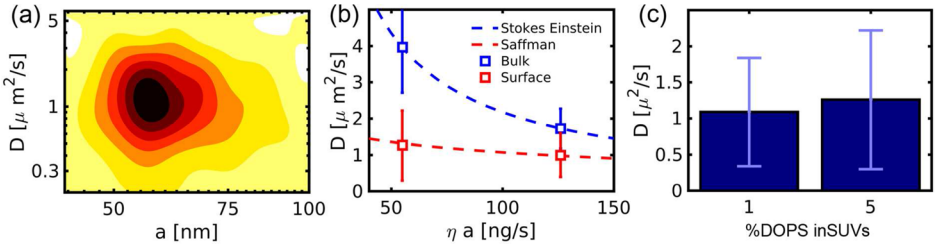

Figure 4. Effect of SUV size, solvent viscosity, and SUV charge density on the vesicle diffusivity. (a) Joint probability density function of vesicle diffusivity D and radius a. The size is reconstructed from the fluorescence intensity. The symmetry of this function indicates that size and diffusivity are uncorrelated. (b) Vesicle diffusivity D versus bulk friction coefficient ηa for freely floating vesicles (blue) and surface-adhering vesicles (red). The dashed lines correspond to the theory for freely floating vesicles (eq 1, blue) and membrane inclusions (eq 2, red). (c) Diffusivity D for membrane-adhering SUVs containing 1 and 5 mol % negatively charged lipids.

cholesterol to an egg phosphatidylcholine (PC) GUV membrane, i.e., from 3.5 to 1.5 μm^2 s^{-1}.[34] This agreement suggests a correlation between the diffusivity of the SUV and that of the underlying membrane. Another possible cause of the observations in Figure 3a would be the presence of cholesterol-enriched domains within the GUV membrane that act as diffusion barriers for the SUVs. In systems where a high-T_m (liquid-crystal−crystalline phase transition temperature) and a low-T_m lipid are mixed with cholesterol (e.g., POPC/sphingomyelin/cholesterol), macroscopic phase separations are readily observable.[35] However, observations of phase separation for a binary phosphocholine/cholesterol system (which is more similar to our study) appear to be ambiguous and dependent on the techniques one employs, and contrasting results have been reported. For instance coexisting fluid domains have not been detected using fluorescence microscopy,[36] but they have been observed using EPR.[37] Hence, elucidating whether phase separation occurs in the 40 mol % cholesterol sample is largely outside the scope of the current study.

To further elucidate the role of the diffusivity of the underlying membrane, we conducted an experiment in which the zwitterionic DOPC lipid in the GUV membrane is replaced with the 1,2-dimyristoyl-*sn*-glycero-3-phosphocholine (DMPC) lipid. As for DMPC (T_m = 24 °C),[38] individual lipids in the GUV membrane are essentially immobile in this experiment (22 °C). Figure 3b shows the SUV trajectories on the DMPC membrane, defined as the SUV angular positions along the rim (θ in Figure 2c) as functions of time. Because the trajectories appear as straight horizontal lines, we conclude that the SUVs are immobile on the DMPC surface. This observation provides strong evidence that the SUV mobility is linked to the lipid mobility in the GUV membrane or more specifically, as demonstrated below, to the viscosity of the GUV membrane.

Our single-vesicle tracking method allows us to study the effect of the vesicle size on SUV diffusivity on the membrane surface. Assuming that the number of fluorescence dye (Rho-PE) molecules is proportional to the SUV surface area, we determine the size of an individual vesicle from the square root of the fluorescence emitted by the vesicle.[39] Figure 4a shows the correlation between the adhering vesicle size and its diffusivity by means of the joint probability density function. The observed symmetry of this function (with a cross correlation of −0.07) indicates a very weak size dependence of the diffusivity of adhering vesicles, which is markedly different from the diffusivity in the bulk, which depends inversely on the size, as given by the Stokes−Einstein relation for particle diffusion in three-dimensional (3D) fluids

$$D = \frac{kT}{6\pi a\eta} \tag{1}$$

where η is the fluid viscosity, a is the particle radius, and kT is the Boltzmann energy. In contrast to hydrodynamics in 3D fluids, the hydrodynamics in (quasi) two-dimensional (2D) fluids, such as bilayers, is relatively size-independent, as predicted by the Saffman− Delbrück model for the diffusivity of membrane inclusions, which is based on the hydrodynamic coupling between the membrane and the surrounding bulk:[40]

$$D = \frac{kT}{4\pi\eta_m}\left(\log\left[\frac{\eta_m}{\eta a}\right] - \gamma\right) \tag{2}$$

Equation 2 adequately describes the diffusion of proteins[41] as well as phase-separated domains[18] within the lipid bilayer and that of lipid clusters associated with externally adhering particles.[22] In eq 2, η and η_m are the viscosities of the solvent and the membrane, respectively, a is the inclusion radius, and $\gamma \approx 0.58$ is Euler's constant. Equation 2 can be regarded as the (pseudo) 2D analog to the Stokes−Einstein relation for particles diffusing in 3D fluids (eq 1), where η_m takes over the role of ηa. In contrast to eq 1, where we have an inverse dependence on particle size, eq 2 reveals a weak logarithmic dependence on size. Note also that the membrane viscosity η_m is closely related to the membrane diffusivity; a large membrane viscosity corresponds to a low membrane diffusivity and vice versa.

An unnoticeable size dependence (Figure 4a) supports the fact that the diffusivity of GUV-riding SUVs is dominated by the membrane viscosity and not by the bulk viscosity. To further verify the inferior role of the bulk viscosity, we increase this quantity by a factor of 2 from 1.0 to 2.3 g m^{-1} s^{-1} by adding 25% (v/v) glycerol to the solvent, which corresponds to a concentration of 3.4 M. Upon adding glycerol, the average diffusivity decreases only 25% from 1.3 ± 1.0 to 1.0 ± 0.6, which is small compared to the 2-fold increase in the viscosity. This confirms that the solvent viscosity plays an inferior role in the diffusivity of adhering vesicles, which, as argued above, is mainly controlled by the viscosity of the underlying membrane. Figure 4b illustrates the contrast in diffusivity between vesicles on the membrane surface and vesicles in the bulk by showing the measured vesicle diffusivity as a function of the bulk friction coefficient ηa. For freely floating vesicles (eq 1), the diffusivity is inversely proportional to this parameter, and the relation for surface-adhering vesicles is much weaker.

The experimental evidence presented above strongly suggests that instead of the bulk viscosity the SUV diffusivity is governed by the viscosity of the underlying GUV membrane η_M. To

DOI: 10.1021/acs.langmuir.6b00985
Langmuir 2016, 32, 5445−5450

validate this hypothesis, we follow the approach presented by Hormel et al.[22] and calculate η_M by inserting measured D into the equation for the diffusivity for membrane inclusions (eq 2). To apply this model, we assume that the mobility of the SUV is coupled to that of a cluster of bound lipids within the GUV membrane. The cluster moves in a surrounding membrane of DOPC/DOEPC (9:1). Because of electrostatic attraction, it is conceivable that the charged DOEPC lipids concentrate in the clusters, which may lower the DOEPC concentration in the surrounding membrane. Given the extremely low coverage of the clusters (they cover a fraction of $\sim 10^{-7}$ of the GUV surface), this effect is negligible and the clusters are assumed to move in a surrounding membrane that is unaffected by the presence of the clusters. Because the cluster is electrostatically bound to the SUV, we suppose that it is within one Debye length of the SUV. For spherically shaped SUVs (radius a) and in the limit $a/\lambda \gg 1$, the radius a_C of this contact area equals (Supporting Information)

$$a_C = \sqrt{2a\lambda} \tag{3}$$

In our system, we have a = 58 nm (Figure S2a) and λ = 4.8 nm (4 mM NaCl), which gives a_C = 23 nm. Inserting this, together with the measured SUV diffusivity $D = 1.3 \pm 1.0\ \mu m^2\ s^{-1}$ into eq 2, we then obtain a membrane viscosity of $\eta_M = (7 \pm 5) \times 10^{-10}$ kg s^{-1}.

This value agrees well with previously found values for DOPC lipids based on fluorescence recovery after photobleaching ($\eta_M = 2 \times 10^{-10}$ kg s^{-1})[15] and based on fluorescence lifetime imaging ($\eta_M = 4 \times 10^{-10}$ kg s^{-1}).[13] The agreement supports the notion that vesicle diffusivity D is described by the theory for membrane inclusions. The applicability of this theory to the present experiment is illustrated in Figure 4b, where we compare eq 2 to the measured diffusivity as a function of the bulk friction coefficient ηa.

The applicability of eq 2 to the present system suggests that each SUV is coupled to a disklike GUV domain, as illustrated in Figure 1b by the red regions. The quasi-2D hydrodynamics of the membrane disk[40] explains the observed size insensitivity of the SUV diffusivity (Figure 4a). Here we present one final control experiment to support this insensitivity. For this purpose, we reduce the fraction of the negatively charged lipids (DOPS) in the SUV membrane 5-fold, i.e., from 5 to 1 mol %. As shown in Figure 4c, this change in the charge density does not appreciably affect the SUV diffusivity, which decreases insignificantly from 1.3 ± 1.0 to $1.1 \pm 0.8\ \mu m^2 s^{-1}$ (Figure 4c). The insensitivity of the diffusivity with respect to the magnitude of the electrostatic attraction is in line with the weak (logarithmic) size dependence in eq 2.

However, since zwitterionic SUVs have a small but measurable negative surface potential,[43] it is possible that increasing the DOPS concentration from 1 to 5 mol % changes the overall surface potential only moderately. To elucidate this, another control experiment was done using SUVs composed of pure zwitterionic DOPC, which were found not to adsorb onto the positively charged GUV surface. Therefore, the negative surface potential of zwitterionic SUVs is expected to be small compared to the potential at 1 mol % DOPS, and changing the DOPS concentration from 1 to 5 mol % changes the overall surface potential substantially.

CONCLUSIONS

We use confocal microscopy to track the motion of electrostatically adhering SUVs riding onto the GUV surface. We find that the SUVs execute 2D Brownian motion, which is insensitive to the solvent viscosity, vesicle radius, vesicle charge density, and vesicle fluidity but is correlated with the fluidity of the underlying GUV membrane instead. Assuming that the adhesion zone defines the size of a disk-shaped inclusion in the GUV membrane, which moves in concert with the SUV, we extract the membrane viscosity within the Saffman−Delbrück framework. Good agreement with previous measurements of membrane viscosity supports the notion that the mobilities of the SUVs are electrostatically linked to that of bound lipid clusters within the target GUV membrane. A major implication of our work is that the electrostatic tethering of small vesicles to cell-sized giant vesicles can divide the diffusional properties of lipid membranes into separate, distinct populations, i.e., clusters of lipids and individual lipids, where the clusters are bound by the SUVs and diffuse slowly within their own milieu (Figure 1b). In this context, it is noted that whereas the Saffman−Delbrück model pertains to the diffusivity of rigid, disk-shaped membrane inclusion, the lipids in the cluster are not necessarily rigidly bound to the SUV but are more likely in dynamic equilibrium with the free lipids in the membrane. Our work also demonstrates that the reversible binding of SUVs to target membranes offers a simple nonperturbative means to measure membrane viscosity, an important parameter whose measurement has long remained challenging.

ASSOCIATED CONTENT

Supporting Information

The Supporting Information is available free of charge on the ACS Publications website at DOI: 10.1021/acs.langmuir.6b00985.

Image analysis and additional supporting figures (Figures S1−S2) and supporting Table 1 (PDF)

Movie (AVI)

Movie (AVI)

AUTHOR INFORMATION

Corresponding Author

*E-mail: njcho@ntu.edu.sg.

Notes

The authors declare no competing financial interest.

ACKNOWLEDGMENTS

We acknowledge support from the National Research Foundation (NRF-NRFF2011-01) and NRF POC and Nanyang Technological University to N.-J.C, and J.C.S.H. acknowledges support from the Provost Office, Nanyang Technological University.

REFERENCES

(1) Seifert, U. Configurations of fluid membranes and vesicles. *Adv. Phys.* **1997**, *46* (1), 13−137.

(2) Lipowsky, R. Generic interactions of flexible membranes. *Handb. Biol. Phys.* **1995**, *1*, 521−602.

(3) Lipowsky, R.; Leibler, S. Unbinding transitions of interacting membranes. *Phys. Rev. Lett.* **1986**, *56* (23), 2541−2544.

(4) Seifert, U.; Lipowsky, R. Adhesion of vesicles. *Phys. Rev. A: At., Mol., Opt. Phys.* **1990**, *42* (8), 4768.

DOI: 10.1021/acs.langmuir.6b00985
Langmuir 2016, 32, 5445−5450

(5) Manz, B. N.; Groves, J. T. Spatial organization and signal transduction at intercellular junctions. *Nat. Rev. Mol. Cell Biol.* **2010**, *11* (5), 342−352.
(6) Grakoui, A.; Bromley, S. K.; Sumen, C.; Davis, M. M.; Shaw, A. S.; Allen, P. M.; Dustin, M. L. The immunological synapse: A molecular machine controlling T cell activation. *Science* **1999**, *285* (5425), 221−227.
(7) Kloboucek, A.; Behrisch, A.; Faix, J.; Sackmann, E. Adhesion-induced receptor segregation and adhesion plaque formation: A model membrane study. *Biophys. J.* **1999**, *77* (4), 2311−2328.
(8) Albersdorfer, A.; Feder, T.; Sackmann, E. Adhesion-induced domain formation by interplay of long-range repulsion and short-range attraction force: A model membrane study. *Biophys. J.* **1997**, *73* (1), 245−257.
(9) Kendall, E. L.; Mills, E.; Liu, J. W.; Jiang, X. M.; Brinker, C. J.; Parikh, A. N. Salt-induced lipid transfer between colloidal supported lipid bilayers. *Soft Matter* **2010**, *6* (12), 2628−2632.
(10) Solon, J.; Pécréaux, J.; Girard, P.; Fauré, M.-C.; Prost, J.; Bassereau, P. Negative tension induced by lipid uptake. *Phys. Rev. Lett.* **2006**, *97* (9), 098103.
(11) Kirchhausen, T. Three ways to make a vesicle. *Nat. Rev. Mol. Cell Biol.* **2000**, *1* (3), 187−198.
(12) Yoshina-Ishii, C.; Chan, Y.-H. M.; Johnson, J. M.; Kung, L. A.; Lenz, P.; Boxer, S. G. Diffusive dynamics of vesicles tethered to a fluid supported bilayer by single-particle tracking. *Langmuir* **2006**, *22* (13), 5682−5689.
(13) Wu, Y.; Štefl, M.; Olzyńska, A.; Hof, M.; Yahioglu, G.; Yip, P.; Casey, D. R.; Ces, O.; Humpolíčková, J.; Kuimova, M. K. Molecular rheometry: direct determination of viscosity in L o and L d lipid phases via fluorescence lifetime imaging. *Phys. Chem. Chem. Phys.* **2013**, *15* (36), 14986−14993.
(14) Honerkamp-Smith, A. R.; Woodhouse, F. G.; Kantsler, V.; Goldstein, R. E. Membrane viscosity determined from shear-driven flow in giant vesicles. *Phys. Rev. Lett.* **2013**, *111* (3), 038103.
(15) Merkel, R.; Sackmann, E.; Evans, E. Molecular friction and epitactic coupling between monolayers in supported bilayers. *J. Phys. (Paris)* **1989**, *50* (12), 1535−1555.
(16) Datta, A.; Pal, S. K.; Mandal, D.; Bhattacharyya, K. Solvation dynamics of coumarin 480 in vesicles. *J. Phys. Chem. B* **1998**, *102* (31), 6114−6117.
(17) Weiß, K.; Neef, A.; Van, Q.; Kramer, S.; Gregor, I.; Enderlein, J. Quantifying the diffusion of membrane proteins and peptides in black lipid membranes with 2-focus fluorescence correlation spectroscopy. *Biophys. J.* **2013**, *105* (2), 455−462.
(18) Cicuta, P.; Keller, S. L.; Veatch, S. L. Diffusion of liquid domains in lipid bilayer membranes. *J. Phys. Chem. B* **2007**, *111* (13), 3328−3331.
(19) Petrov, E. P.; Petrosyan, R.; Schwille, P. Translational and rotational diffusion of micrometer-sized solid domains in lipid membranes. *Soft Matter* **2012**, *8* (29), 7552−7555.
(20) Dimova, R.; Dietrich, C.; Hadjiisky, A.; Danov, K.; Pouligny, B. Falling ball viscosimetry of giant vesicle membranes: finite-size effects. *Eur. Phys. J. B* **1999**, *12* (4), 589−598.
(21) Lee, G. M.; Ishihara, A.; Jacobson, K. A. Direct observation of Brownian motion of lipids in a membrane. *Proc. Natl. Acad. Sci. U. S. A.* **1991**, *88* (14), 6274−6278.
(22) Hormel, T. T.; Kurihara, S. Q.; Brennan, M. K.; Wozniak, M. C.; Parthasarathy, R. Measuring lipid membrane viscosity using rotational and translational probe diffusion. *Phys. Rev. Lett.* **2014**, *112* (18), 188101.
(23) Angelova, M. I.; Dimitrov, D. S. Liposome electroformation. *Faraday Discuss. Chem. Soc.* **1986**, *81*, 303−311.
(24) Morales-Penningston, N. F.; Wu, J.; Farkas, E. R.; Goh, S. L.; Konyakhina, T. M.; Zheng, J. Y.; Webb, W. W.; Feigenson, G. W. GUV preparation and imaging: minimizing artifacts. *Biochim. Biophys. Acta, Biomembr.* **2010**, *1798* (7), 1324−1332.
(25) Brändén, M.; Tabaei, S. R.; Fischer, G.; Neutze, R.; Höök, F. Refractive-index-based screening of membrane-protein-mediated transfer across biological membranes. *Biophys. J.* **2010**, *99* (1), 124−133.
(26) Filipe, V.; Hawe, A.; Jiskoot, W. Critical evaluation of Nanoparticle Tracking Analysis (NTA) by NanoSight for the measurement of nanoparticles and protein aggregates. *Pharm. Res.* **2010**, *27* (5), 796−810.
(27) Lei, G.; MacDonald, R. C. Lipid bilayer vesicle fusion: intermediates captured by high-speed microfluorescence spectroscopy. *Biophys. J.* **2003**, *85* (3), 1585−1599.
(28) Kunze, A.; Svedhem, S.; Kasemo, B. Lipid transfer between charged supported lipid bilayers and oppositely charged vesicles. *Langmuir* **2009**, *25* (9), 5146−5158.
(29) Saxton, M. J.; Jacobson, K. Single-particle tracking: applications to membrane dynamics. *Annu. Rev. Biophys. Biomol. Struct.* **1997**, *26* (1), 373−399.
(30) Lee, Y. K.; Kim, S.; Oh, J.-W.; Nam, J.-M. Massively Parallel and Highly Quantitative Single-Particle Analysis on Interactions between Nanoparticles on Supported Lipid Bilayer. *J. Am. Chem. Soc.* **2014**, *136* (10), 4081−4088.
(31) Sagle, L. B.; Ruvuna, L. K.; Bingham, J. M.; Liu, C.; Cremer, P. S.; Van Duyne, R. P. Single plasmonic nanoparticle tracking studies of solid supported bilayers with ganglioside lipids. *J. Am. Chem. Soc.* **2012**, *134* (38), 15832−15839.
(32) Calamai, M.; Pavone, F. S. Single molecule tracking analysis reveals that the surface mobility of amyloid oligomers is driven by their conformational structure. *J. Am. Chem. Soc.* **2011**, *133* (31), 12001−12008.
(33) Ewers, H.; Jacobsen, V.; Klotzsch, E.; Smith, A. E.; Helenius, A.; Sandoghdar, V. Label-free optical detection and tracking of single virions bound to their receptors in supported membrane bilayers. *Nano Lett.* **2007**, *7* (8), 2263−2266.
(34) Rubenstein, J.; Smith, B. A.; McConnell, H. M. Lateral diffusion in binary mixtures of cholesterol and phosphatidylcholines. *Proc. Natl. Acad. Sci. U. S. A.* **1979**, *76* (1), 15−18.
(35) Veatch, S. L.; Keller, S. L. Miscibility phase diagrams of giant vesicles containing sphingomyelin. *Phys. Rev. Lett.* **2005**, *94* (14), 148101.
(36) Veatch, S. L.; Keller, S. L. Seeing spots: complex phase behavior in simple membranes. *Biochim. Biophys. Acta, Mol. Cell Res.* **2005**, *1746* (3), 172−185.
(37) Sankaram, M. B.; Thompson, T. E. Cholesterol-induced fluid-phase immiscibility in membranes. *Proc. Natl. Acad. Sci. U. S. A.* **1991**, *88* (19), 8686−8690.
(38) Needham, D.; Evans, E. Structure and mechanical properties of giant lipid (DMPC) vesicle bilayers from 20. degree. C below to 10. degree. C above the liquid crystal-crystalline phase transition at 24. degree. C. *Biochemistry* **1988**, *27* (21), 8261−8269.
(39) Kunding, A. H.; Mortensen, M. W.; Christensen, S. M.; Stamou, D. A fluorescence-based technique to construct size distributions from single-object measurements: application to the extrusion of lipid vesicles. *Biophys. J.* **2008**, *95* (3), 1176−1188.
(40) Saffman, P. Brownian motion in thin sheets of viscous fluid. *J. Fluid Mech.* **1976**, *73* (04), 593−602.
(41) Peters, R.; Cherry, R. J. Lateral and rotational diffusion of bacteriorhodopsin in lipid bilayers: experimental test of the Saffman-Delbrück equations. *Proc. Natl. Acad. Sci. U. S. A.* **1982**, *79* (14), 4317−4321.
(42) Stanich, C. A.; Honerkamp-Smith, A. R.; Putzel, G. G.; Warth, C. S.; Lamprecht, A. K.; Mandal, P.; Mann, E.; Hua, T.-A. D.; Keller, S. L. Coarsening dynamics of domains in lipid membranes. *Biophys. J.* **2013**, *105* (2), 444−454.
(43) Voinov, M. A.; Rivera-Rivera, I.; Smirnov, A. I. Surface electrostatics of lipid bilayers by EPR of a pH-sensitive spin-labeled lipid. *Biophys. J.* **2013**, *104* (1), 106−116.

DOI: 10.1021/acs.langmuir.6b00985
Langmuir 2016, 32, 5445−5450